Nonclinical Antiangiogenesis and Antitumor Activities of Axitinib (AG-013736), an Oral, Potent, and Selective Inhibitor of Vascular Endothelial Growth Factor Receptor Tyrosine Kinases 1, 2, 3

Dana D. Hu-Lowe, Helen Y. Zou, Maren L. Grazzini, Max E. Hallin, Grant R. Wickman, Karin Amundson, Jeffrey H. Chen, David A. Rewolinski, Shinji Yamazaki, Ellen Y. Wu, Michele A. McTigue, Brion W. Murray, Robert S. Kania, Patrick O'Connor, David R. Shalinsky, and Steve L. Bender

Abstract

Purpose: Axitinib (AG-013736) is a potent and selective inhibitor of vascular endothelial growth factor (VEGF) receptor tyrosine kinases 1 to 3 that is in clinical development for the treatment of solid tumors. We provide a comprehensive description of its *in vitro* characteristics and activities, *in vivo* antiangiogenesis, and antitumor efficacy and translational pharmacology data.

Experimental Design: The potency, kinase selectivity, pharmacologic activity, and antitumor efficacy of axitinib were assessed in various nonclinical models.

Results: Axitinib inhibits cellular autophosphorylation of VEGF receptors (VEGFR) with picomolar IC_{50} values. Counterscreening across multiple kinase and protein panels shows it is selective for VEGFRs. Axitinib blocks VEGF-mediated endothelial cell survival, tube formation, and downstream signaling through endothelial nitric oxide synthase, Akt and extracellular signal-regulated kinase. Following twice daily oral administration, axitinib produces consistent and dose-dependent antitumor efficacy that is associated with blocking VEGFR-2 phosphorylation, vascular permeability, angiogenesis, and concomitant induction of tumor cell apoptosis. Axitinib in combination with chemotherapeutic or targeted agents enhances antitumor efficacy in many tumor models compared with single agent alone. Dose scheduling studies in a human pancreatic tumor xenograft model show that simultaneous administration of axitinib and gemcitabine without prolonged dose interruption or truncation of axitinib produces the greatest antitumor efficacy. The efficacious drug concentrations predicted in nonclinical studies are consistent with the range achieved in the clinic. Although axitinib inhibits platelet-derived growth factor receptors and KIT with nanomolar *in vitro* potencies, based on pharmacokinetic/pharmacodynamic analysis, axitinib acts primarily as a VEGFR tyrosine kinase inhibitor at the current clinical exposure.

Conclusions: The selectivity, potency for VEGFRs, and robust nonclinical activity may afford broad opportunities for axitinib to improve cancer therapy.

The vascular endothelial growth factor (VEGF)/VEGF receptor tyrosine kinase (RTK) signaling pathway plays a pivotal role in tumor angiogenesis by promoting vascular and lymphatic endothelial cell proliferation, survival, and invasion, resulting in neovascularization, tumor growth, and metastasis (1–4). Many antiangiogenic agents including multi-RTK inhibitors (RTKI) are either approved or are being tested in clinical trials. Sunitinib [anti-VEGF, platelet-derived growth factor receptors (PDGFR), KIT, and Flt-3] is Food and Drug Administration approved for the treatment of advanced renal cell carcinoma (5) and imatinib-refractory gastrointestinal stromal tumors (6) and is in phase III development across multiple tumor types. Sorafenib (anti-VEGFR, PDGFR, b-Raf, Flt-3, and KIT) is approved for the treatment of advanced metastatic renal cell carcinoma (7) and for the first-line treatment of advanced hepatocellular carcinoma,[1] whereas it had limited activity in advanced non-small cell lung cancer (8). In addition, bevacizumab (anti-VEGF-A monoclonal antibody) is approved for the treatment of first-line colorectal cancer in combination with 5-fluorouracil-based regimens (9), for subgroups of advanced non-small cell lung cancer in combination with paclitaxel/carboplatin (10), and recently for late-stage breast cancer in combination with Taxol (11). Several other RTKIs with varying

Authors' Affiliation: PGRD-La Jolla, Pfizer, Inc., San Diego, California
Received 3/18/08; revised 6/25/08; accepted 7/8/08.
The costs of publication of this article were defrayed in part by the payment of page charges. This article must therefore be hereby marked *advertisement* in accordance with 18 U.S.C. Section 1734 solely to indicate this fact.
Note: Supplementary data for this article are available at Clinical Cancer Research Online (http://clincancerres.aacrjournals.org/).
Requests for reprints: Dana D. Hu-Lowe, Department of Cancer Biology, PGRD-La Jolla, Pfizer, 10646 Science Center Drive, San Diego, CA 92121. Phone: 858-622-6019; Fax: 858-622-5999; E-mail: dana.hu-lowe@pfizer.com.

doi:10.1158/1078-0432.CCR-08-0652

[1] http://www.press.bayer.com/baynews/baynews.nsf/id/A7DF79054835DC96C1257398003C9BC5/$File/2007-0641E.rtf, accessed June 18, 2008.

Translational Relevance

Axitinib is a potent and selective VEGFR inhibitor currently in phase II/III development. Clinical reports and narrowly focused academic publictions have been published. There is a need to describe the characteristics of axitinib based on information of discovery and translational research. *Clinical Cancer Research* is an ideal journal for this article because its broad audience of medical oncologists, translational researchers, and basic research scientists can all benefit from this comprehensive and integrated report. The translational value fo the article includes the clinically relevant target and efficacious concentrations; the nature of axitinib's selectivity in the context of the current clinical dose; the molecular basis for clinical hypertension and why it would be manageable; the potential impact of dose scheduling, interruption, or truncation on antitumor efficacy; and for the first time the proof of concept of enhanced benefit by targeting both the VEGF ligand and intracellular VEGFR of tumor vasculature – a hypothesis that is being tested in the clinic. We also briefly discuss the difference in selectivity profile between several similar RTKIs, an issue of interest in the field of antiangiogenesis. This discussion provides clarification on why we believe axitinib would present non-overlapping and important therapeutic opportunities in the clinic.

VEGFR selectivity are in phase II/III development with some activities including PTK787 (12), AZD2171 (13), and motesanib diphosphate (14). The phase II activities of multi-RTKIs XL999 [ref. 15; anti-fibroblast growth factor receptors (FGFR) 1-3, VEGFR-2, PDGFR, RET, KIT, SRC, and Flt-3] and XL880 (ref. 16; anti-MET and VEGFR) are encouraging but are coupled with noticeable toxicities.

Although the multi-RTKIs can be highly effective in treating cancers through antagonizing more than one cancer pathway, an oral, potent, and selective VEGF RTKI with desirable pharmacokinetics may improve effectiveness, ease of dose adjustment, and high combinability with chemotherapy and targeted therapy, which enables the treatment of a broad spectrum of cancers. Furthermore, the highly potent and selective VEGF RTKIs may afford to avoid significant adverse events in patients that do not tolerate the inhibition of multiple RTKs (often expressed on epithelial cells, hematopoietic lymphocytes, and/or leukocytes), as in the case of potent, selective, and prolonged PDGFR inhibition that may not be desirable (17, 18).

Axitinib is an oral, potent, and selective small-molecule inhibitor of VEGF RTKs 1, 2, 3. It is currently in phase I to III development in a range of solid tumors. In nonclinical and clinical studies, the compound has been shown to inhibit angiogenesis, vascular permeability, and blood flow (19–21). In phase II studies, axitinib showed single-agent activity in a wide range of tumor types, including advanced renal cell carcinoma (22), thyroid cancer (23), non-small cell lung cancer (24), and melanoma (25) as well as improved progression-free survival and overall survival in advanced and metastatic pancreatic cancer when combined with gemcitabine (26). In addition, axitinib has a well-tolerated clinical safety profile and a relatively shorter half-life (2-5 h). Compared with some other similar antiangiogenic agents currently in development, axitinib appears to be a much more potent and selective VEGFR inhibitor (Fig. 1), which may be a key contributing factor to its clinical activity and tolerability.

Materials and Methods

Compound synthesis and formulation

Axitinib (*N*-methyl-2-[3-(*E*)-2-pyridin-2-yl-vinyl-1*H*-indazol-6-ylsulfanyl]benzamide) was synthesized as described in U.S. Patent 6,534,524. For *in vitro* experiments, axitinib was dissolved in 10 mmol/L DMSO and diluted as needed, and for *in vivo* studies, axitinib was formulated in 0.5% carboxymethylcellulose/H_2O·HCl (g/v, pH 2-3) and dosed as a suspension at 5 mL/kg orally twice daily. Bevacizumab (Avastin; Henry Shein) was formulated in sterile PBS and dosed at 5 mg/kg i.v. twice a week. Docetaxel (Taxotere; Amersham/Bergen Brunswick) was administered i.v. at 5 to 40 mg/kg once a week. Carboplatin was dosed i.p. daily for 5 days during each treatment cycle. Gemcitabine (Eli Lilly) was formulated in 0.9% NaCl and dosed i.p. 3 times per d for 4 d with a 10-day dosing break between cycles.

Cells and cell culture

Human umbilical vein endothelial cells (HUVEC) were purchased from Clonetics or Cambrex Bio Science. Human microvascular endothelial cells were purchased from Cascade Biologics. MV522 (human colon cancer) cells were obtained from the University of California. M24met (human melanoma) cells were provided by Dr. Barbara Mueller (La Jolla Institute for Molecular Medicine). Tumor cell lines LLC (murine Lewis lung carcinoma), NIH-3T3 (murine fibroblastoma), C6 (rat glioblastoma), U87MG (human glioblastoma), MDA-MB-231 (human breast carcinoma), HT29 (human colon carcinoma), A375 and A2058 (human melanoma), NCI-H526 (human small cell lung carcinoma), A2780 (human ovarian carcinoma), and Namalwa (human lymphoma) were obtained from the American Type Culture Collection.

Animals

Female *nu/nu* mice or severe combined immunodeficient beige mice (ages 7-10 weeks) were obtained from Harlan or Charles River Laboratories. Animals were fed Lab Diet 5061 (PMI Nutrition International) and water *ad libitum*. Animal experiments were carried out in observance with Pfizer Institutional Animal Care and Use Committee guidelines and in accordance with the Guide for the Care and Use of Laboratory Animals (ILARCLS, 1996) by Institute of Laboratory Animal Research (NIH).

Cellular receptor kinase phosphorylation assay

Porcine aorta endothelial (PAE) cells overexpressing full-length VEGFR-2, PDGFR-β, KIT, and NIH-3T3 overexpressing murine VEGFR-2 (Flk-1) or PDGFR-α were generated as described previously (27, 28). The ELISA capture plates were prepared by coating 96-well ReactiBind plates (Pierce) with 100 μL/well of 2.5 μg/mL anti-VEGFR-2 antibody (Novus Biologicals), 0.75 μg/mL anti-PDGFR-β antibody, 0.25 μg/mL anti-PDGFR-α antibody (both Santa Cruz Biotechnology), 0.5 μg/mL anti-KIT antibody (NeoMarkers), or 1.20 μg/mL anti-Flk-1 antibody (Invitrogen). Measurement of RTK phosphorylation by ELISA was done as described previously (29).

Three-dimensional spheroidal tube formation assay

Five hundred human microvascular endothelial cells were added to EGM-2 medium containing 0.24% methylcellulose and transferred to U-bottomed 96-well plates to form a spheroid overnight. Approximately 50 spheroids were collected and mixed with 2 mg/mL fibrinogen solution containing 4% to 8% fetal bovine serum (FBS)

with or without compound in the 48-well plates coated with thrombin (5,000 units/mL). The resulting three-dimensional fibrin gel was covered with EGM-2 containing 4% to 8% FBS and incubated at 37°C. Endothelial tube formation was observed daily under an inverted microscope.

Immunoprecipitation and immunoblotting

Endothelial or tumor cells were starved for 18 h in the presence of either 1% FBS (HUVEC) or 0.1% FBS (tumor cells). Axitinib was added and cells were incubated for 45 min at 37°C in the presence of 1 mmol/L Na_3VO_4. The appropriate growth factor was added to the cells, and after 5 min, cells were rinsed with cold PBS and lysed in the lysis buffer (Cell Signaling) and a protease inhibitor cocktail (Roche Applied Science). The lysates were incubated with immunoprecipitation antibodies for the intended proteins overnight at 4°C. Antibody complexes were conjugated to protein A beads and supernatants were separated by SDS-PAGE. The Super Signal West Dura kit (Pierce) was used to detect the chemiluminescent signal.

In vivo target modulation

VEGFR-2 phosphorylation inhibition in the rat development model. Six-day-old Sprague-Dawley rats (Charles River Laboratory) were given two i.p. injections of axitinib. Animals were sacrificed, retinas were collected and lysed, and immunoprecipitation/immunoblotting experiments were done as described above. ECL-Plus (Amersham Pharmacia Biotech) was used for detection and densitometry analysis was done using the Alpha Imager 8800 (Alpha Innotech).

VEGFR-2 phosphorylation inhibition in xenograft tumors. Mice with M24met xenograft tumors (400-600 mm^3) were administered with a single dose of axitinib or the control (0.5% carboxymethylcellulose/H_2O). Blood and tumor tissue samples were collected for pharmacokinetic and VEGFR-2 measurements. Total protein concentrations in tumor tissues were determined using the Bradford colorimetric assay (Bio-Rad). Procedures for immunoprecipitation/immunoblotting and ELISA were as described above.

Axitinib pharmacokinetics

Plasma concentrations of axitinib were quantitatively determined by a triple-quadruple mass spectrometer equipped with a high-performance liquid chromatography system (Agilent 1100) using a Phenyl column (Zorbax Eclipse XDB, 5 μm particle size, 50 × 2.1 mm) under isocratic conditions of 60:40 water/acetonitrile containing 0.1% formic acid. Data were collected under multiple reaction monitoring mode of m/z 387.3→356.2 for axitinib and m/z 394.2→360.2 for the internal standard, AG-013736-d7. The method quantified for axitinib over the range of 1 to 1,000 ng/mL in mouse plasma. The area under the plasma concentration-time curve of axitinib was calculated using the linear trapezoidal rule.

Skin vascular permeability assay in naive or tumor-bearing mice

The assay was done according to Miles and Miles (30) with some modifications. *nu/nu* mice (n = 5-8) received a single oral dose of axitinib followed by an injection of 30 μL Evan's blue dye through the tail vein. Thirty minutes later, murine VEGF-A (400 ng in 10 μL PBS) or PBS was injected into the trunk area posterior to the shoulder of the animal. Four hours later, the skin region immediately surrounding the blue color area was dissected and immersed in 1 mL formamide. Evan's blue was extracted by incubating the tissues in formamide at 56°C for 24 h. Vascular permeability was quantified by measuring light absorbance at 620 nm.

Mouse xenograft models

In general, tumor cells in FBS-depleted medium were implanted s.c. into the right flank region of athymic mice, except for the following: the M24met cells were implanted intradermally in a 50 to 100 μL volume in BALB/C severe combined immunodeficient mice; the procedures for orthotopic implantation of HCT-116-GFP and SN12C-GFP tumors have been described elsewhere (31); the A375 cells were implanted in the presence of 10% Matrigel; the LLC tumors were inoculated either using the suspension cells or 2 × 2 mm viable tumor fragments via the Trocar needles. Unless otherwise specified, mice were randomized when the average tumor was ~100 mm^3 (9-12 per group). Tumor volumes

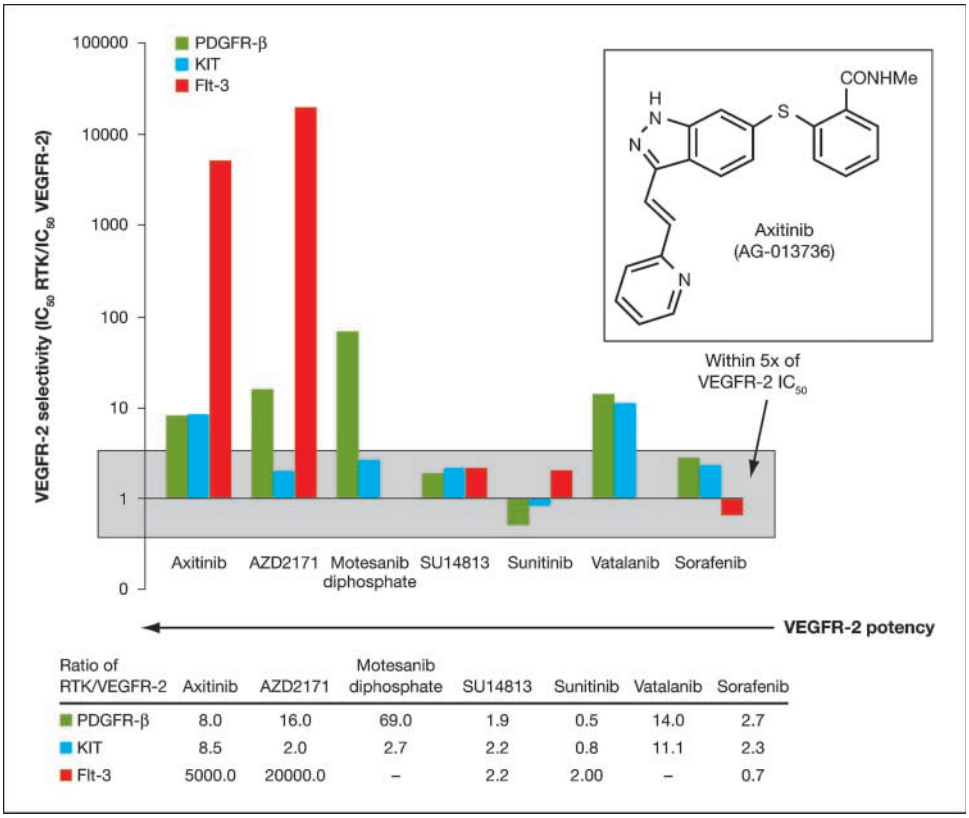

Ratio of RTK/VEGFR-2	Axitinib	AZD2171	Motesanib diphosphate	SU14813	Sunitinib	Vatalanib	Sorafenib
PDGFR-β	8.0	16.0	69.0	1.9	0.5	14.0	2.7
KIT	8.5	2.0	2.7	2.2	0.8	11.1	2.3
Flt-3	5000.0	20000.0	–	2.2	2.00	–	0.7

Fig. 1. Comparison of cellular selectivity of approved and investigational small-molecule RTKIs. Data are expressed as ratios of IC_{50} of RTK/IC_{50} of VEGFR-2, where cellular IC_{50} values for axitinib, sunitinib, SU14813, and vatalanib were obtained from receptor phosphorylation assays using transfected PAE cells; the ratios for sorafenib, motesanib diphosphate (AMG706), and AZD2171 were calculated based on published data. Ratio of IC_{50} of RTK/IC_{50} of VEGFR-2 ≤ 5 is indicated by the gray panel, suggesting lack of a meaningful selectivity for VEGFRs versus a given RTK (PDGFR-β, KIT, or Flt-3). *Inset,* chemical structure of axitinib.

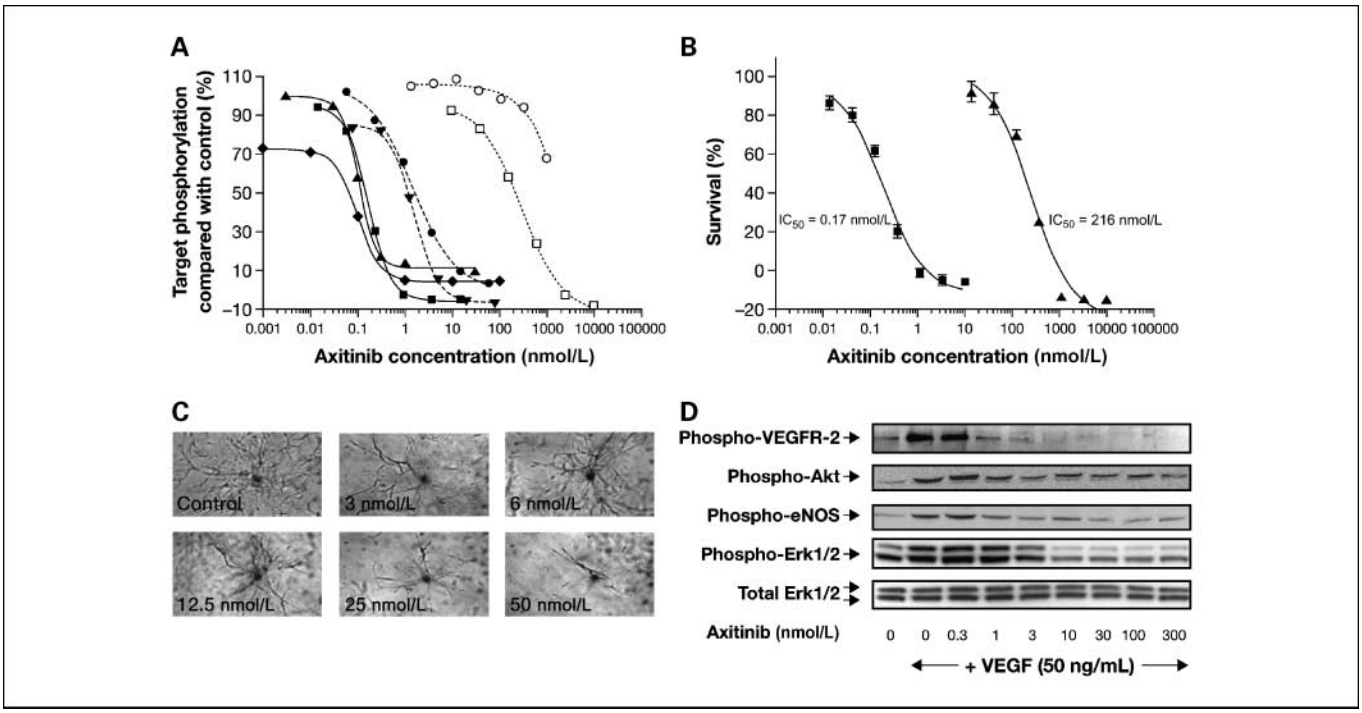

Fig. 2. Cellular potency and selectivity of axitinib. *A,* axitinib preferentially inhibits cellular phosphorylation of VEGFR-1, VEGFR-2, and VEGFR-3. The graph presents an overlay of dose-response curves generated from ELISA (VEGFR-2, PDGFR-β, KIT, FGFR-1, and Flt-3) and immunoprecipitation/immunoblotting (VEGFR-1 and VEGFR-3) assays. After treatment with axitinib across the designated concentration range at 37°C for 1 h, cells were stimulated for 5 to 10 min with 50 to 100 ng/mL VEGF-A for VEGFR-1 (▲) and VEGFR-2 (■), 100 ng/mL VEGF-C for VEGFR-3 (♦), 20 to 50 ng/mL PDGF-BB for PDGFR-β (●), 80 ng/mL SCF for KIT (▼), 50 ng/mL basic FGF for FGFR-1 (□), or 100 ng/mL Flt-3 ligand for Flt-3 (○; all from R&D Systems). The rest of the procedures are described in Materials and Methods. The IC_{50} values were calculated by fitting the data using a four-variable analysis in a statistical data-analyzing template. *B,* dose-dependent inhibition of VEGF-stimulated but not basic FGF-stimulated HUVEC survival. HUVECs (passages 4-5) were incubated with axitinib for 45 min before adding 20 ng/mL VEGF (■) or basic FGF (▲). Three days later, viable cell numbers were determined by the method of MTT. Mean ± SD of triplicates. IC_{50} values were calculated the same as above. *C,* axitinib (3, 6, 12.5, 25, and 50 nmol/L) dose-dependently blocked the sprouting and tube formation of human microvascular endothelial cell spheroids. Images were captured on day 7 by a digital camera (Olympus BX60) connected to the microscope. *D,* dose-dependent inhibition of Akt, eNOS, and ERK1/2 phosphorylation by axitinib in HUVEC by immunoprecipitation/immunoblotting. HUVECs were starved and treated with axitinib for 45 min with the indicated concentrations followed by a 5-min VEGF stimulation. The cell lysates (1 mg total lysate proteins) were immunoprecipitated with antibody SC-1158 (Santa Cruz Biotechnology) for VEGFR-2. For immunoblotting, anti-phosphotyrosine antibody 4G10, phospho-Akt, phospho-eNOS, and phospho-MAPK$^{44/42}$ (all Cell Signaling) were used for phosphorylated VEGFR-2, Akt, eNOS, and ERK1/2, respectively. The horseradish peroxidase-linked IgG was used as the secondary antibody to probe for phosphorylated proteins. Total VEGFR-2, Akt, eNOS, and ERK were also probed using antibodies specific to these molecules. The levels of cellular proteins were not changed as a result of axitinib treatment (data not shown). Equal protein loading of each lane is indicated by total ERK1/2 signal (*bottom row*).

were measured three times per week by electronic calipers and calculated according to the following equation: $0.5 \times [\text{length} \times (\text{width})^2]$. Treatment usually lasted for 2 to 4 weeks or until tumors reached 1,500 mm^3. The procedure for tumor bioluminescent imaging and quantification using the IVIS Imaging System (Xenogen) has been reported elsewhere (32).

Immunohistology studies

CD31 immunohistochemistry fluorescent staining. Frozen slides of tumors were fixed in acetone for 10 min, air dried, washed in PBS, and blocked in 5% rabbit serum (Vector Laboratories)/PBS for 30 min at room temperature. The samples were exposed to rat anti-mouse CD31 (clone 13.3; BD Bioscience) at 1:150 dilution in 5% rabbit serum/PBS for 1 h at room temperature. The slides were washed in PBS three times, and fluorescently conjugated secondary antibodies, Alexa Fluor 594 rabbit anti-goat (Invitrogen), were diluted 1:100 in PBS/0.05% Tween 20 and incubated on the slides for 20 min at room temperature. Tumor samples were washed again in PBS three times before being mounted in Vectashield (Hard Set mounting medium with 4′,6-diamidino-2-phenylindole; Vector Labs). Images were captured with a Zeiss Axiovert 200M, a ×20 optical objective lens, and an Axiocam HR color digital camera.

Caspase-3 and Ki-67 staining. The tumor samples (4-5 per group) were formalin-fixed, processed in Tissue Tek Vacuum Infiltration Processor (Sakuka, Finetek USA), and embedded in paraffin wax (Surgipath Medical Industries). Sections (5 μm) were cut and baked on to microscope slides. All staining was run on a Discovery XT autostainer and visualized with DAB Map Kit (both from Ventana Medical Systems). Stained sections were imaged using a BX60 Olympus microscope and a Microfire Digital Camera (Olympus).

Results

***Axitinib potently inhibits cellular VEGF RTK activities* in vitro.** In transfected or endogenous RTK-expressing cells, axitinib potently blocked growth factor-stimulated phosphorylation of VEGFR-2 and VEGFR-3 with average IC_{50} values of 0.2 and 0.1 to 0.3 nmol/L, respectively (Fig. 2A; Table 1). Cellular activity against VEGFR-1 was 1.2 nmol/L (measured in the presence of 2.3% bovine serum albumin), equivalent to an absolute IC_{50} of ~0.1 nmol/L, based on protein binding of axitinib. The potency against murine VEGFR-2 (Flk-1) in Flk-1-transfected NIH-3T3 cells was 0.18 nmol/L, similar to that of its human homologue. Axitinib showed ~8- to 25-fold higher IC_{50} against the closely related type III and V family RTKs, including PDGFR-β (1.6 nmol/L), KIT (1.7 nmol/L), and PDGFR-α (5 nmol/L; Table 1); nanomolar concentrations of axitinib blocked PDGF BB-mediated human glioma U87MG cell (PDGFR-β-positive) migration but not proliferation (data not shown). In contrast,

Table 1. Enzymatic K_i and cellular IC_{50} values determined by receptor phosphorylation assays

Target	RTK phosphorylation, IC_{50} (nmol/L) ± SD	
	ELISA*	Immunoprecipitation/immunoblotting †
VEGFR-2 (KDR)	0.20 ± 0.06 (VEGFR-2/PAE)	0.06 (HUVEC)
VEGFR-1 (Flt-1)	ND	~0.1 ‡ (HUVEC)
Murine VEGFR-2 (Flk-1)	0.18 ± 0.03 (Flk-1/NIH-3T3)	ND
VEGFR-3	ND	0.1 ~ 0.3 (VEGFR-3/PAE)
PDGFR-β	1.6 ± 0.4 (PDGFR-β/PAE)	2.9 ‡ (NIH-3T3)
PDGFR-α	5.0 ± 1.0 (PDGFR-α/NIH-3T3)	ND
KIT	1.7 ± 0.6 (KIT/PAE)	0.98 ‡ (NCI-H526)
CSF-1R	73 ± 18 (CSF-1R/NIH-3T3)	ND
Flt-3	>1,000 (RS;411)	ND

*Abbreviation: ND, not determined.
Measured in the presence of 0.1% FBS.
† Measured in the presence of 1% FBS (HUVEC) or 0.1% FBS (PAE or tumor cells).
‡ Measured in the presence of 1% FBS and 2.3% bovine serum albumin. Data were corrected for protein binding with the consideration that the presence of 2.3% bovine serum albumin typically shifted cellular IC_{50} values up by a factor of ~10.

axitinib had much weaker target and functional activity against FGFR-1 (Fig. 1A and B; Table 1). With up to 1 μmol/L concentrations, axitinib showed minimal activity against Flt-3 in RS;411 cells and RET in TT cells (data not shown). A similar trend was observed for enzymatic inhibitory activity (K_i) against recombinant tyrosine kinases of the aforementioned receptors (data not shown). Importantly, axitinib had little inhibition against "off-target" protein kinases; at a concentration of 1 μmol/L (~1,000-fold of the K_i for VEGFR-2) across three kinase panels of ~100 protein kinases (Pfizer in-house; Upstate and Dundee panels), axitinib inhibited only five protein kinases: Abl, Aurora-2, Arg, AMPK, Axl, and MST2 (≥60% inhibition). Finally, axitinib exhibited no significant activity in a broad protein kinase screen (Cerep; data not shown).

Axitinib inhibits VEGF-mediated endothelial cell survival, migration, and tube formation. Axitinib showed potent inhibition of VEGF-stimulated but not basic FGF-stimulated HUVEC survival with ~1,000-fold selectivity for VEGFR-2 versus FGFR-1 receptors (Fig. 2B). The average IC_{50} value for VEGFR-2 derived from the functional assays (0.24 ± 0.09 nmol/L) was similar to that obtained in the cellular receptor phosphorylation assays (Table 1), confirming that receptor antagonism led to a functional inhibition by the compound. In addition, axitinib dose-dependently inhibited spheroidal endothelial tube formation in a three-dimensional fibrin matrix system (Fig. 2C; Supplementary Fig. S1). Higher compound concentrations than other types of assays were required to inhibit tube formation because of the presence of the higher serum level (4-8% FBS) in the system.

Axitinib inhibits intracellular signal transduction in endothelial cells. Axitinib rapidly and dose-dependently reduced the phosphorylation of Akt, endothelial nitric oxide synthase (eNOS), and extracellular signal-regulated kinase 1/2 (ERK1/2), key downstream signaling molecules of VEGF (Fig. 2D), with IC_{50} values similar to that of the inhibition of VEGFR-2. This suggests that the reduction in Akt, eNOS, and ERK1/2 phosphorylation may be due to antagonism of upstream VEGFRs by axitinib.

Target modulation* in vivo *by axitinib. Acute axitinib treatment rapidly and significantly reduced retinal vascular VEGFR-2 phosphorylation. One hour after the second dose, retinal VEGFR-2 phosphorylation was reduced by 80% to 90% compared with that of the control tissues (Fig. 3A, *left*). Six and 24 to 32 h post-dose, the phospho-VEGFR-2 levels returned to ~50% and 100% of the control, respectively. Levels of phospho-VEGFR-2 inversely correlated with axitinib plasma concentrations over the study time course. The EC_{50} value for the inhibition of VEGFR-2 phosphorylation was 0.49 nmol/L (or 0.19 ng/mL, the unbound value corrected for plasma protein binding; Fig. 3A, *right*).

Axitinib also inhibited murine VEGFR-2 phosphorylation in angiogenic vessels of xenograft tumors of the M24met; M24met tumors secrete high VEGF-A, are highly vascularized, and do not express functional human VEGFR-2. A single oral dose of axitinib (100 mg/kg) markedly suppressed murine VEGFR-2 phosphorylation for up to 7 h compared with control tumors (Fig. 3B). Phosphorylation of downstream ERK1/2 was also measured from the same samples. Compared with the control, partial inhibition of ERK1/2 signal was observed in treated tissues as early as 30 min post-dose and remained inhibited for at least 7 h (Fig. 3C).

Axitinib rapidly inhibited VEGF-induced vascular permeability in the skin of mice; the inhibition was dose-dependent and directly correlated with drug concentration in mice (Fig. 3D). Pharmacokinetic/pharmacodynamic analysis indicated an unbound EC_{50} of 0.46 nmol/L (Supplementary Fig. S2). Similar inhibitory effects were also shown in the skin of MV522 tumor-bearing mice without exogenous VEGF-A stimulation (data not shown).

Taken together, the required *in vivo* pharmacologic concentration (C_{target}) based on the inhibition of vascular VEGFR-2 phosphorylation and VEGF-mediated permeability is ~0.5 nmol/L (unbound), which translates to a C_{target} of ~100 nmol/L (or 40 ng/mL, total concentration) in humans.

Axitinib inhibits tumor growth and angiogenesis in mice. Axitinib inhibited the growth of human xenograft tumors in mice (Table 2). Axitinib produced dose-dependent growth delay regardless of initial tumor size, model type, or implant site. Importantly, axitinib exhibited primary tumor inhibition and distant metastasis control in orthotopically implanted tumors such as M24met (melanoma), HCT-116 (colorectal cancer), and SN12C (renal cell carcinoma). A dose-dependent

growth inhibition in the MV522 tumor model is shown (Fig. 4A). Tumor growth inhibition (TGI) was associated with central necrosis, reduction in microvessel density (CD31 staining) and Ki-67, and increased caspase-3 in the tumor (Fig. 4B; Supplementary Fig. S3). Similar effects were observed in all tumor types examined regardless of tumor type and RTK expression. In summary, axitinib treatment produced consistent antitumor efficacy across various tumor types and this activity is associated with reduction in vascular angiogenesis and tumor proliferation and increase in tumor apoptosis.

Determination of ED_{50} and C_{eff}. The efficacious dose resulting in 50% antitumor efficacy (ED_{50}) was determined

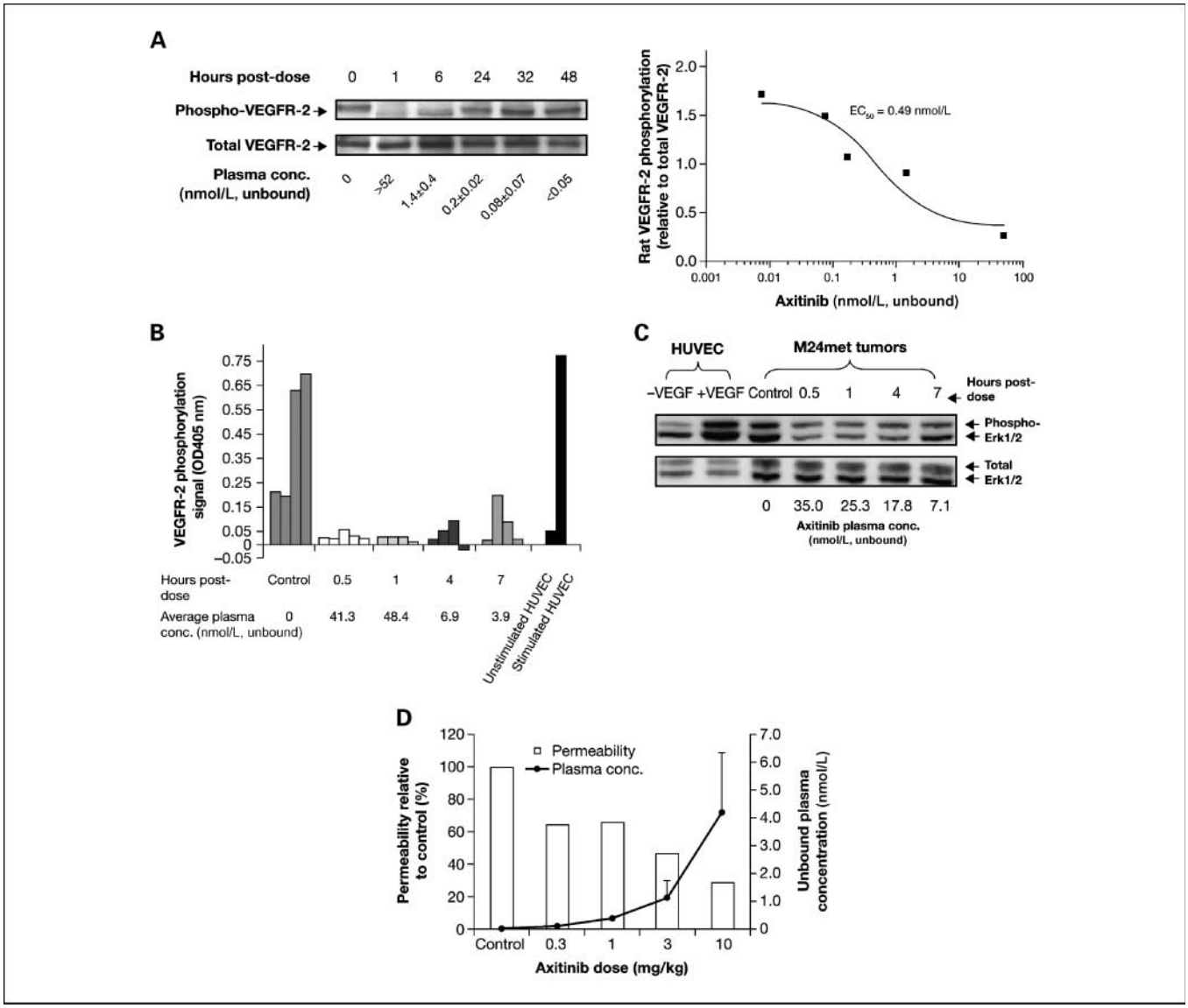

Fig. 3. Axitinib showed *in vivo* target modulation and antiangiogenesis. *A, in vivo* modulation of VEGFR-2 phosphorylation in the rat ocular angiogenesis model. Six-week-old rats were given two injections of axitinib (30 mg/kg i.p.). Animals were sacrificed at 0, 1, 6, 24, 32, and 48 h post-dose and six retinas from three animals were pooled and lysed. Soluble retinal protein (1 mg) was immunoprecipitated with VEGFR-2 antibody (Santa Cruz Biotechnology) and separated by SDS-PAGE. *Left,* phospho-VEGFR-2 and total VEGFR-2 were probed using anti-phosphotyrosine antibody and VEGFR-2 antibody (both Santa Cruz Biotechnology), respectively. *Right,* relative VEGFR-2 phosphorylation signals were normalized to total VEGFR-2 intensities in the corresponding lanes and plotted against plasma concentrations at the time points of tissue collection; a nonlinear regression curve fit of the plot revealed the target inhibition concentration of 0.49 nmol/L (unbound; 0.19 ng/mL). For curve fit purpose, the 48 h plasma concentration is assumed to be 0.05 nmol/L (unbound), which is right below the detection limit. *B, in vivo* modulation of VEGFR-2 phosphorylation in the vasculature of M24met xenograft tumors in mice. M24met cells (2×10^6) were implanted into the lower flank region of severe combined immunodeficient (BALB/c) mice intradermally. A single dose of axitinib (50 mg/kg orally) was given when tumors reached 500 to 800 mm^3. Animals were sacrificed at 0.5, 1, 4, and 7 h post-dose (n = 4-5 per group) and blood samples were collected for plasma concentration. Tumor samples were harvested and lysates (1-2 mg total tumor or HUVEC proteins) were added with 4 to 10 μg antibody to VEGFR-2 (SC-1158) for immunoprecipitation. The remaining procedure is the same as described previously. Shown are phosphorylation signals for all individual samples from treatment time point, the control group, and HUVECs. Average plasma concentration values are also indicated. *C, in vivo* inhibition of ERK1/2 in M24met tumors. Change of ERK1/2 activity of the M24met tumors in response to axitinib treatment were measured in tumor lysates. Total lysates were separated by SDS-PAGE and probed with anti-phospho-$MAPK^{44/42}$ or anti-$MAPK^{44/42}$ (Cell Signaling). The remaining procedure is the same as described previously in Materials and Methods. Each lane is a representative tumor under each time point of tissue collection and the corresponding plasma concentration values are indicated. *D,* axitinib treatment reduced skin vascular permeability, which inversely correlated to plasma drug concentrations. Vascular permeability values of VEGF-stimulated and axitinib-treated groups (0.3, 1, 3, and 10 mg/kg) were measured as described in Materials and Methods. Group vascular permeability was normalized to that of the control group (*Y axis, left*) and plotted against dose levels. The corresponding plasma concentration values at 4 h post-dose are also plotted against dose levels [shown as group mean ± SD] (*Y axis, right*).

Table 2. Summary of single-agent antitumor efficacy of axitinib in nonclinical models

Disease type	Description	Dose (mg/kg)	Regimen	Size at start of dosing (mm^3)	Dosing period (d)	TGI (%)
Colon carcinoma	Dose-dependent TGI in MV522 model	1	orally twice daily	170	16	18.3
		3				15.2
		10				63.9
		30				61.1
		100				80.3
		150				94.6
		200				96.3
	Dose response TGI in HT29 model	10	orally twice daily	110	16	51
		30				76
		100				99
		150				99
	TGI in orthotopic HTC-116 GFP model	30	orally twice daily	1 d after implant	10	Unevaluable
					17	87
					28	80
Lung	Dose-dependent efficacy in LLC model	1	orally twice daily	<50	18	33
		3				49
		10				75
		30				68
		100				69
		300				Not tolerated
	TGI and antimetastasis activity and survival assessment in LLC model	100	orally twice daily	Prophylactic dose (s.c. model)	38	63
			orally twice daily	Tail vein implanted tumors	Survival	~11 d median survival vs control
	TGI in KIT^+ NCI-H526 SCLC model	30	orally twice daily	180	13	47
		100				61
Melanoma	TGI in established A375 melanoma	10	orally twice daily	336	12	38
		30				59
	Dose-dependent TGI in activating mutant b-Raf A2058 melanoma model	3	orally twice daily	150	15	36
		10				57
		30				65
		100				83
Renal carcinoma	TGI in orthotopically implanted SN12C GFP human renal carcinoma model	10	orally twice daily	2 d after implant	41	54
		10			72	61
		30			41	56
		30			72	74
		100			41	63
		100			72	70
Glioma	Dose-dependent efficacy in U87 glioma model	10	orally twice daily	46-72	17	44
		30				69
		60				74
NHL	Efficacy in human lymphoma model	50	orally twice daily	1 d after implant	14	Significant reduction in i.p. tumor burden as indicated by reduction in body weights
		50			22	
	Namalwa (time course)	50			23	

NOTE: TGI (%) was calculated according to the equation: $[1 - \Delta Treat/\Delta Control] \times 100$, where $\Delta Treat$ and $\Delta Control$ are changes of tumor volume between the end of the dosing and the beginning of the dosing for a treated group and a control group, respectively.

using the MV522 model. MV522 tumor cells do not express functional VEGF or PDGF RTKs. In addition, the tumors have a moderate growth rate, making it an ideal model to evaluate the antiangiogenesis-associated ED_{50} of axitinib. Based on the relationship between dose and the corresponding TGI (Fig. 4A), the ED_{50} was determined to be 8.8 mg/kg twice daily (Supplementary Fig. S4) and a 30 mg/kg twice daily dose level corresponded to an ED_{70} in this model. The range of *in vivo* efficacious concentration (C_{eff}) corresponding to a 50% TGI was determined by evaluating the relationship between TGI (Fig. 4A) and plasma concentrations. Based on C_{min} (trough concentration), the estimated unbound C_{eff} was determined to be 0.28 nmol/L (or 0.11 ng/mL; Fig. 4C, *left*); based on C_{ave} (average concentration across 24 h), the calculated unbound C_{eff} was determined to be 0.85 nmol/L (0.33 ng/mL; Fig. 4C, *right*). Thus, the C_{eff} value range (0.28-0.85 nmol/L) is in agreement with the C_{target} value (0.5 nmol/L) obtained from *in vivo* target modulation studies.

The relationship between dose and target inhibition was further analyzed based on pharmacokinetic profiles, IC_{50} values,

C_{target}, and C_{eff}. Plasma concentrations at 10 mg/kg (ED_{50} dose) and 30 mg/kg (ED_{70} dose) were both above and near C_{target} (for VEGFRs) and C_{eff} (TGI-based) during the majority of the day (Fig. 4D). However, the plasma concentrations at these doses only allowed a total of ~5 and 12 h coverage over the cellular IC_{50} of PDGFR-β, respectively (anti-PDGFR-based C_{target} or C_{eff} from *in vivo* studies is not available). Based on this analysis, the antitumor efficacy at 10 mg/kg in the MV522 model (VEGFR-null, PDGFR-null) appeared to be mainly driven from vascular VEGFR inhibition by axitinib. In the same model, infusions of axitinib achieved a near maximal antitumor efficacy (80%) that was associated with a steady-state plasma concentration greater than the cellular IC_{50} for VEGFRs but below the cellular IC_{50} for PDGFR-β (data not shown).

Axitinib enhances antitumor efficacy of chemotherapeutic agents in multiple tumor models. The antitumor efficacy of axitinib was assessed in combination with docetaxel (in LLC and human breast cancer models), carboplatin (in a human

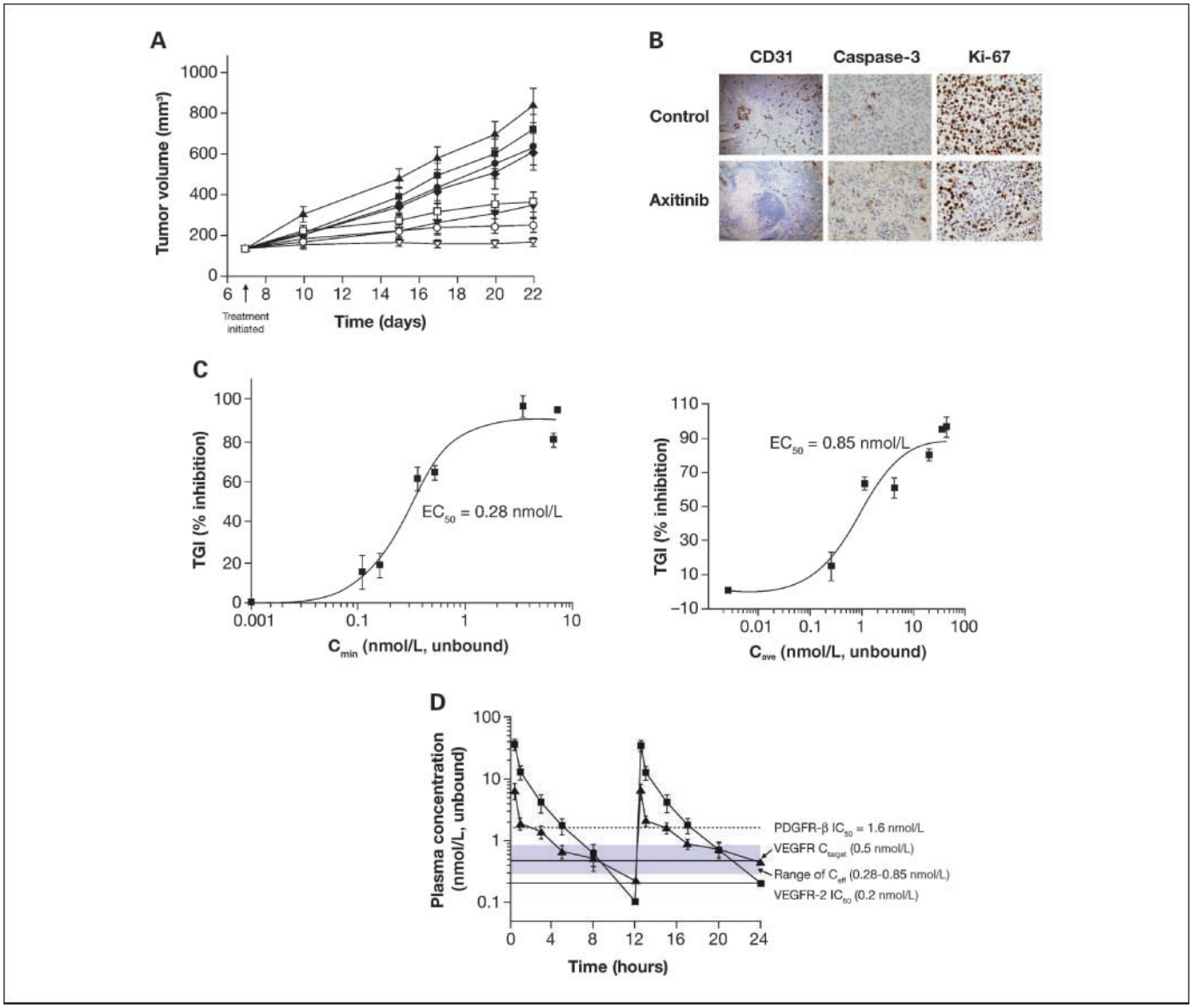

Fig. 4. Antitumor efficacy and pharmacokinetic/pharmacodynamic correlation of axitinib. *A,* axitinib dose-dependent inhibition of tumor growth in MV522. Tumor cells (2×10^6) were inoculated into the right upper flank of *nu/nu* mice. Tumors were randomized according to tumor size and axitinib treatment was initiated on day 7. Mean ± SE. ■, control; ▲, axitinib 0.3 mg/kg; ♦, axitinib 1 mg/kg; ●, axitinib 3 mg/kg; ▼, axitinib 10 mg/kg; □, axitinib 30 mg/kg; ○, axitinib 100 mg/kg; ▽, axitinib 150 mg/kg. *B,* axitinib inhibition of microvessel growth compared with the control as shown by CD31 staining (clone Mec 13.3; PharMingen). Highly positive vessel staining (*brown*) is shown in the control group compared with the axitinib-treated group. Axitinib treatment also induced the level of caspase-3 and reduced Ki-67 staining in MV522 tumors. Antibody 9661L (Cell Signaling) and RM9106 (Lab Vision/NeoMarkers) were used as the primary antibodies for caspase-3 and Ki-67, respectively. All images were taken at ×20 magnification. *C,* derivation of EC_{50} of axitinib from the MV522 TGI study. The %TGI ± SE was plotted against either C_{min} (*left*) or C_{ave} (*right*) plasma concentrations corresponding to the different dose levels to derive EC_{50}. Curve fit and calculation of EC_{50} values using the sigmoidal dose-response nonlinear regression model (Prism, GraphPad) are shown. To facilitate the curve fit, a close to 0% TGI was assigned to an artificial plasma concentration of 1/100 of the lowest measurable value. The curve fit was nonrestrictional at the high concentration end (a 100% TGI was not enforced for curve fit). *D,* axitinib preferentially inhibited VEGFRs at the ED_{50} and ED_{70} doses. The pharmacokinetic profile is created by plotting the plasma concentrations (± SE) against the time points of treatment at 10 mg/kg twice daily (▲) and 30 mg/kg twice daily (■). The pharmacokinetic profile was analyzed against the derived C_{target} (0.5 nmol/L) and C_{eff} (0.28-0.85 nmol/L) of axitinib. IC_{50} values for VEGFR-2 (0.2 nmol/L) and PDGFR-β (1.6 nmol/L) are also shown. The duration of action against VEGFRs and PDGFR-β is assessed base on this correlative analysis.

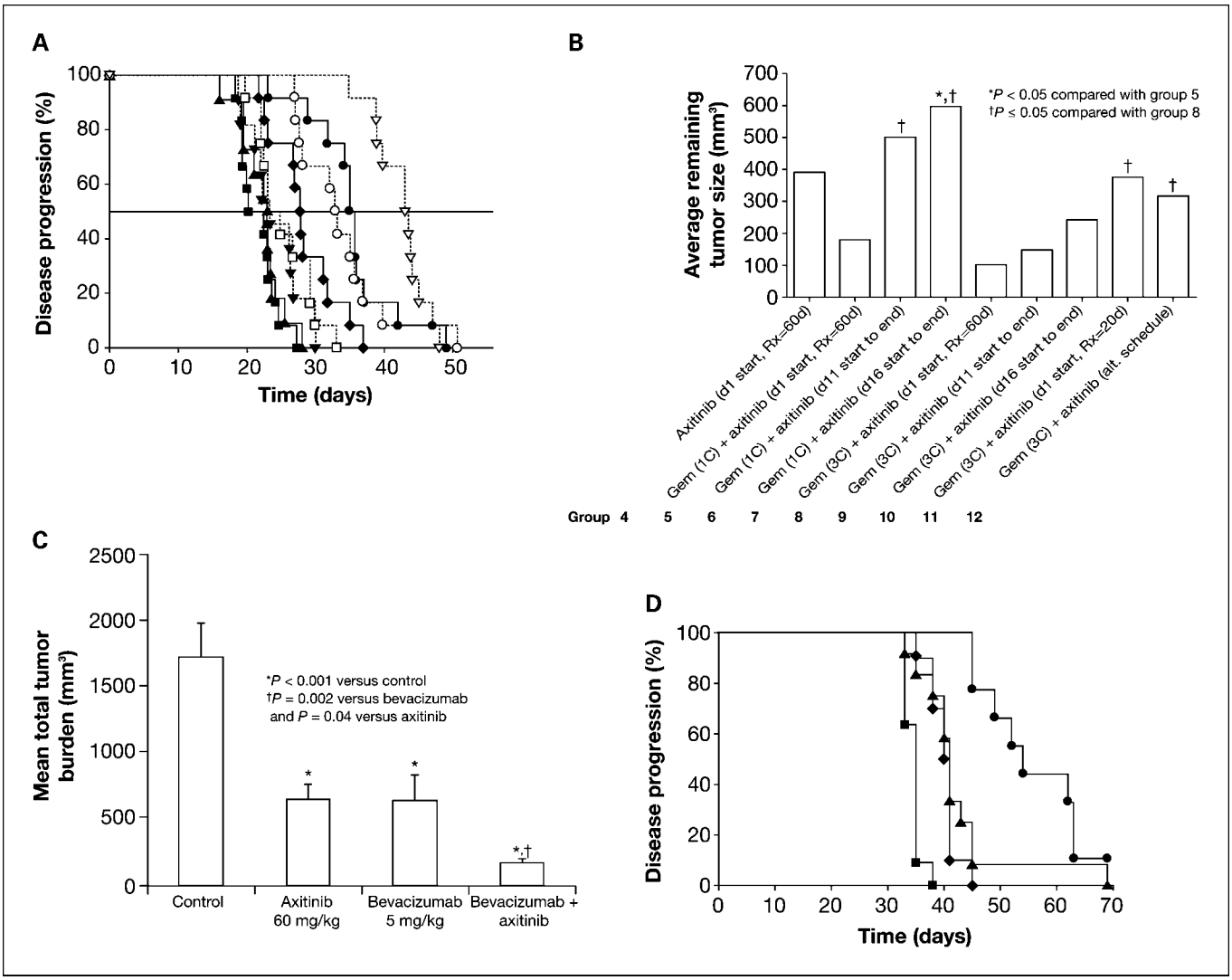

Fig. 5. Effect of axitinib in combination with chemotherapeutics and bevacizumab. *A,* axitinib significantly enhanced animal survival as single agent and in combination with docetaxel in the LLC model. LLC cells were inoculated into B6D2F1 mice (1×10^6 per site, s.c.). Mice were randomly assigned to treatment with axitinib alone, docetaxel alone (40 mg/kg; ▼), or axitinib plus docetaxel combination treatment. The Kaplan-Meier plot shows delay of TTE; ΔTTE (TTE_{treat} - $TTE_{control}$) was found to be 1.9 d for docetaxel alone ($P > 0.05$, versus vehicle control; ■), 1.5 d ($P > 0.05$, versus control), 6.4 d ($P < 0.001$, versus control), and 13.9 d ($P < 0.001$, versus control) for axitinib at 3 mg/kg (▲), 10 mg/kg (♦), and 30 mg/kg (●), respectively. ΔTTE was 2.5 d ($P = 0.05$, versus axitinib; $P = 0.6$, versus docetaxel), 11.6 d ($P = 0.047$, versus axitinib; $P < 0.001$, versus docetaxel), and 21.9 d ($P = 0.043$, versus axitinib; $P < 0.001$, versus docetaxel) for the combination treatment groups involving docetaxel and axitinib of 3 mg/kg (□), 10 mg/kg (○), and 30 mg/kg (▽), respectively. *B,* dose scheduling study of axitinib and gemcitabine in human pancreatic carcinoma model BxPC-3. Xenografts were initiated by s.c. implanting a ~1 mm^3 BxPC-3 tumor fragment in the right flank of each mouse. Treatments began when tumors were ~90 mm^3 in size. Axitinib was dosed at 30 mg/kg orally twice daily for 60 d (*60 d*) except for the last two groups; gemcitabine (*Gem*) was given at 140 mg/kg i.p. 3 times per day for 4 d for either one cycle (*1C*) or three cycles (*3C)*. Tumors were measured twice weekly and animals were euthanized when their tumors reached an endpoint volume of 1,200 mm^3 or on 60 d of treatment, whichever came first. Data shown are tumor sizes at 53 d of treatment. The control and gemcitabine single groups are not included because all tumors in these groups reached the 1,200 mm^3 end point before day 53. Statistical significance was determined by ANOVA with a Tukey's multiple comparison test. *C,* combination therapy of axitinib and bevacizumab significantly inhibited spontaneous lymph node metastasis and prolonged survival of animals in the M24met model. Primary tumors were surgically removed once they reached the size of 200 to 300 mm^3, which enhanced tumor metastasis to lymph nodes and the lung. Lymph node tumors were measured until the predetermined survival end point (total lymph node tumor size = 2,000 mm^3). Treatment with axitinib (60 mg/kg orally twice daily), bevacizumab (5 mg/kg i.v., 2xqw), or the combination of the two agents began 1 d post-surgery and continued until the end of the study. Lymph node tumor volume comparison after 33-day treatments is shown. Mean ± SE. *D,* a Kaplan-Meier plot showed significant delay of disease progression with combination therapy compared with either single-agent alone. Combination group (●) $P < 0.0001$, versus axitinib (60 mg/kg; ♦) and $P = 0.0076$, versus bevacizumab (5 mg/kg; ▲). ■, control.

ovarian cancer model), or gemcitabine (in a human pancreatic cancer model). These models were chosen because they have only low or moderate sensitivity to chemotherapies in mice.

In the LLC model, axitinib (10 or 30 mg/kg orally twice daily) in combination with a maximally tolerated dose of docetaxel (40 mg/kg once a week) enhanced tumor growth delay, defined as the increase in the median time to the end point (TTE) in a treatment group compared with the control group. A TTE (a measure of disease progression) is defined as tumor size = 1,500 mm^3 or animal moribund due to tumor burden or metastasis. A 54% or 100% tumor growth delay was obtained for docetaxel plus 10 or 30 mg/kg axitinib versus a 9%, 30%, and 60% for docetaxel alone and 30 and 60 mg/kg axitinib alone, respectively (data not shown). Docetaxel plus axitinib significantly delayed disease progression compared with docetaxel alone (Fig. 5A). In the MDA-MB-435/HAL-luc

model, axitinib (30 mg/kg) and docetaxel (5 mg/kg; 25% of murine maximally tolerated dose) produced a robust tumor growth delay as shown by the reduction of tumor bioluminescent signal (Supplementary Fig. S5) and increase in the number of complete responders compared with either single agent alone (data not shown).

The antitumor efficacy of axitinib in combination with gemcitabine was investigated against various dosing schedules in the gemcitabine-resistant BxPC-3 human pancreatic cancer model (Fig. 5B). In one study, single-agent gemcitabine (140 mg/kg i.p., days 1, 4, 7, and 10, either one-cycle or three-cycle treatments) or axitinib (30 mg/kg orally twice daily) delayed tumor growth. In the groups receiving gemcitabine plus axitinib, the "early dosing" of axitinib (day 1, group 5) produced a greater tumor growth delay than "late dosing" [starting axitinib on day 11 (group 6) or 16 (group 7) after initiation of gemcitabine] regardless of the number of gemcitabine cycles; with the same axitinib regimen, three gemcitabine treatment cycles (group 8, 9, 10) produced a greater efficacy than one gemcitabine treatment cycle (group 5, 6, 7). Alternating dose of the two agents (group 12) or early termination of axitinib (group 11) resulted in a significant compromise in tumor growth delay compared with coadministration and continuous twice daily dosing of axitinib.

Combination of axitinib and bevacizumab produced significant antimetastasis activity in M24met model. The ability of axitinib to enhance bevacizumab efficacy in the orthotopically implanted and spontaneous metastasis human melanoma M24met tumor model was investigated; M24met tumors do not express functional RTKs (data not shown). Most importantly, circulating human VEGF-A, the ligand for bevacizumab, was found to be >95% of total circulating VEGF-A *in vivo* in this model.

In this study, both axitinib (60 mg/kg orally twice daily) and bevacizumab (5 mg/kg i.v., 2xqw) exhibited moderate single-agent activity against lymph node tumor metastasis. The combination of the two agents significantly improved antimetastasis efficacy assessed based on reduction of lymph node tumor mass (Fig. 5C), antiangiogenesis (Supplementary Fig. S6), and proliferation index of metastatic lymph node tumors (Supplementary Fig. S7). In addition, the combination therapy significantly prolonged animal survival measured by reduction of time to progression (TTE), with a 13-day TTE for both single agents versus the control and a 20-day TTE for combination therapy versus the control (Fig. 5D). As expected, dosing with bevacizumab or bevacizumab plus axitinib, but not axitinib single-agent treatment, significantly reduced free plasma human VEGF-A (data not shown).

Discussion

Axitinib was generated from an iterative structure-based drug design approach and is a potent (picomolar) and selective inhibitor of VEGF RTKs 1, 2, 3. The compound exhibits ~8-fold lower inhibitory activity against PDGFRs and KIT and has little activity against other type III and V family kinases (CSF-1R, Flt-3, FGFR-1, and RET), epidermal growth factor receptor, and c-Met. Axitinib is highly selective against nonreceptor kinases and proteins in a variety of off-target screening assays.

Axitinib dose-dependently inhibits endothelial cell proliferation, survival, and three-dimensional tube formation *in vitro*. Axitinib rapidly blocks downstream signal transduction via the eNOS/Akt pathway that has been implicated in the pathologic angiogenesis and normal vascular homeostasis (33, 34). The required concentrations for eNOS and Akt phosphorylation inhibition track with that for VEGFR-2 phosphorylation inhibition by axitinib. Furthermore, phospho-eNOS inhibition was reversible with the signal fully recovered soon after (1-2 h) withdrawal of axitinib (whereas inhibition of phospho-VEGFR-2 was sustained for up to 8 h; data not shown). Consistent with these findings is the observation that, in the clinic, axitinib-associated increases in diastolic blood pressure are reversible and closely correlate with clinical outcome (35).

In vivo, axitinib markedly inhibited vascular VEGFR-2 phosphorylation in (*a*) the development rat ocular angiogenesis model, (*b*) the VEGF-mediated skin permeability model of mice, and (*c*) the vasculature of a human xenograft tumor model in mice. In addition, the C_{target} values derived from the rat ocular angiogenesis model and the mouse permeability model ($\sim$0.5 nmol/L) are consistent with the efficacy-based C_{eff} value (0.28-0.85 nmol/L) obtained from TGI studies. Furthermore, the C_{eff} value derived from these nonclinical studies in general agrees with the range of plasma concentrations of the 5 mg twice daily clinical starting dose of axitinib (C_{ave} = 0.19 $\pm$ 0.12 nmol/L; interim data). This clinical dose is associated with reduced tumor permeability and blood flow (19), tumor shrinkage (RECIST), overall response rate, and survival benefit observed in multiple phase II axitinib single-agent and combination studies in the clinic (22–25).

Axitinib alone produced marked antitumor efficacy that was associated with antiangiogenesis effects across nonclinical models regardless of the RTK expression profile in the tumor cells. This may imply that axitinib may have broad indications and utility in the clinic. In addition, based on published information and this report, we believe that vascular VEGFR inhibition alone by axitinib is essential and sufficient to produce significant antiangiogenesis and meaningful antitumor activity. In animal models, this activity can be achieved with a 10 to 15 mg/kg orally twice daily administration of axitinib. Higher dose levels of axitinib (>30 mg/kg) in mice have been shown to produce a C_{max} exposure significantly above the IC_{50} for PDGFR and typically were associated with greater antitumor efficacy (see Fig. 4A); we believe that although a transient PDGFR inhibition may have partially contributed to the efficacy, a more sustained and prolonged inhibition of VEGFR-2 throughout the majority of the day played a significant role in efficacy enhancement. The latter is consistent with the preliminary nonclinical data that equal or even greater efficacy can be achieved through continuous infusion of axitinib with a steady-state plasma concentration lower than PDGFR IC_{50}. Furthermore, in the RIP-Tag2 transgenic tumor model in which axitinib at efficacious dose levels (up to 25 mg/kg) produced rapid and dramatic inhibition of tumor endothelial cell fenestration, VEGFR-2 expression, vessel growth, and vascular density but did not decrease PDGFR expression or tumor vasculature-associated pericytes, there was, however, evidence that certain markers on the pericytes were modulated (36, 37). The interpretation of the latter remains to be addressed. Based on our nonclinical and clinical pharmacokinetic/pharmacodynamic understanding, C_{max} of the current clinical starting dose of axitinib (5 mg twice daily) in general does not exceed the IC_{50} for PDGFR in the majority

of patients; this suggests that the observed clinical activity of axitinib in most patients is driven by inhibition of VEGFR activity.

Combining axitinib with docetaxel generated marked suppression of disease progression compared with docetaxel alone in a docetaxel-resistant LLC model. In addition, additive or synergistic enhancement of TGI and response to chemotherapeutic agents alone was observed when axitinib was combined with docetaxel, carboplatin, and gemcitabine. With gemcitabine, dose scheduling was an important contributing factor to efficacy. This may indicate that simultaneous administration of both compounds without prolonged dose interruptions or withdrawal as of axitinib is likely to produce the optimal clinical outcome. More studies are under way to gain a deeper insight into how axitinib and chemotherapeutic agents can be best used for maximal activity in animal models.

Dose-escalation studies showed that axitinib single agent had a therapeutic index of 64 in the murine LLC model (data not shown). In general, chronic treatments (3-6 weeks) of axitinib up to 100 mg/kg in combination with maximally tolerated dose levels of chemotherapeutic agents were tolerated in tumor-bearing mice, consistent with the highly selective nature of axitinib. In addition, the nonclinical safety profile was extensively evaluated in safety pharmacology, genetic toxicology, and general toxicology assessments and the monitorable and manageable toxicity profile supported the clinical evaluation of axitinib.

In the clinic, bevacizumab (anti-VEGF-A) has shown activity in combination with chemotherapeutics (9, 10). Currently, several clinical studies are being conducted combining bevacizumab with small-molecule RTKIs to determine whether clinical activity may be improved. Here, we present data from a nonclinical model to address this hypothesis. In a spontaneous metastatic human melanoma model, we observed that coadministration of axitinib and bevacizumab significantly improved antimetastasis efficacy compared with either agent alone. Lymph node metastasis of M24met may be highly dependent on lymphangiogenesis, in which VEGF-C/VEGFR-3 plays a central role (38–41). In addition to VEGF-A, other ligands including VEGF-D (42), VEGF-E (43, 44), and PlGF (45–47) are found to contribute to tumor angiogenesis and progression by binding to VEGFR-3, VEGFR-1, VEGFR-2, or neuropilin (48). Furthermore, these growth factors interact with each other synergistically to promote processes leading to sustained tumor progression (45, 46). In this context, small-molecule VEGF RTKIs may have advantage over VEGF-A-selective bevacizumab. Finally, a recent report showed that intracellular autonomous VEGF/VEGFR-2 signaling had an indispensable role in vascular homeostasis and endothelial cell survival (49) and that intracellular VEGFR-2 activation in wild-type cells was suppressed by a small-molecule VEGFR antagonist but not by bevacizumab. The implication of intracellular VEGFR-2 inhibition in the context of tumor angiogenesis remains to be elucidated; however, it is conceivable that membrane permeable axitinib, but not bevacizumab, may potently inhibit intracellular VEGFR-2 signaling (in addition to inhibiting VEGFR autophosphorylation mediated by exogenous VEGF) in tumor endothelial cells that ultimately induce endothelial cell apoptosis that cannot be rescued by exogenous VEGF. Although clinically combining axitinib and bevacizumab may not be feasible due to overlapping mechanism-based adverse events such as hypertension, we believe that, in principle, combining intracellular and extracellular inhibition of VEGF signaling would lead to robust and prolonged antiangiogenesis.

In summary, axitinib is a potent and selective inhibitor of VEGFR-1, VEGFR-2, and VEGFR-3 with proven antitumor activity from nonclinical and clinical studies. Axitinib may evolve to become one of the most promising oral VEGF RTKIs with significant single-agent antitumor activity and combinability for the treatment of a broad spectrum of human malignancies.

Disclosure of Potential Conflicts of Interest

No potential conflict of interest were disclosed.

Acknowledgments

We thank Jingchuan Zhang, Roslyn Dillon, Qiuhua Li, Ming Qiu, Min-Jean Yin, Enhong Chen, Lianglin Zhang, Celin Tompkins, Auzon Acena, Davina Heller, Alicia Shelley, Sylvia Vekich, Michelle Herrmann, David Romero, Young Kim, Jim Solowiej, Shawn Misialek, the Piedmont Research Center, and AntiCancer for technical assistance; Diane Matsumoto, Tatiana Koudriakova, Barbara Mroczkowski, and Gerrit Los for valuable support and discussions; Department of Comparative Medicine (Pfizer) for animal husbandry support; Dr. Barbara M. Mueller (La Jolla Institute for Molecular Medicine) for kindly providing the M24met cells and for technical expertise in the model; Drs. Kari Alitalo (University of Helsinki) and Barry Nelkin (Johns Hopkins University) for testing potency of axitinib against VEGFR-3 and RET, respectively; and ACUMED for assistance with manuscript preparation funded by Pfizer.

References

1. Ferrara N, Gerber HP, LeCouter J. The biology of VEGF and its receptors. Nat Med 2003;9:669–76.
2. Bergers G, Benjamin LE. Tumorigenesis and the angiogenic switch. Nat Rev Cancer 2003;3:401–10.
3. Ferrara N. Role of vascular endothelial growth factor in the regulation of angiogenesis. Kidney Int 1999;56:794–814.
4. Folkman J. Tumor angiogenesis: therapeutic implications. N Engl J Med 1971;285:1182–6.
5. Motzer RJ, Hutson TE, Tomczak P, et al. Sunitinib versus interferon α in metastatic renal-cell carcinoma. N Engl J Med 2007;356:115–24.
6. Demetri GD, van Oosterom AT, Garrett CR, et al. Efficacy and safety of sunitinib in patients with advanced gastrointestinal stromal tumour after failure of imatinib: a randomised controlled trial. Lancet 2006;368:1329–38.
7. Escudier B, Eisen T, Stadler WM, et al. Sorafenib in advanced clear-cell renal-cell carcinoma. N Engl J Med 2007;356:125–34.
8. Gatzemeier U, Blumenschein G, Fosella F, et al. Phase II trial of single-agent sorafenib in patients with advanced non-small cell lung carcinoma [abstract]. J Clin Oncol 2006;24 Suppl:364s.
9. Hurwitz H, Fehrenbacher L, Novotny W, et al. Bevacizumab plus irinotecan, fluorouracil, and leucovorin for metastatic colorectal cancer. N Engl J Med 2004;350:2335–42.
10. Sandler A, Gray R, Perry MC, et al. Paclitaxel-carboplatin alone or with bevacizumab for non-small-cell lung cancer. N Engl J Med 2006;355:2542–50.
11. Miller K, Wang M, Gralow J, et al. Paclitaxel plus bevacizumab versus paclitaxel alone for metastatic breast cancer. N Engl J Med 2007;357:2666–76.
12. Wood JM, Bold G, Buchdunger E, et al. PTK787/ZK 222584, a novel and potent inhibitor of vascular endothelial growth factor receptor tyrosine kinases, impairs vascular endothelial growth factor-induced responses and tumor growth after oral administration. Cancer Res 2000;60:2178–89.
13. Wedge SR, Kendrew J, Hennequin LF, et al. AZD2171: a highly potent, orally bioavailable, vascular endothelial growth factor receptor-2 tyrosine kinase inhibitor for the treatment of cancer. Cancer Res 2005;65:4389–400.
14. Polverino A, Coxon A, Starnes C, et al. AMG 706, an oral, multikinase inhibitor that selectively targets vascular endothelial growth factor, platelet-derived growth factor, and Kit receptors, potently inhibits angiogenesis and induces regression in tumor xenografts. Cancer Res 2006;66:8715–21.

15. Cripe L, McGuire W, Wertheim M, et al. Integrated report of the phase 2 experience with XL999 administered IV to patients (pts) with NSCLC, renal cell CA (RCC), metastatic colorectal CA (CRC), recurrent ovarian CA, acute myelogenous leukaemia (AML), and multiple myeloma (MM) [abstract]. J Clin Oncol 2007;25 Suppl:160s.

16. Ross RW, Stein M, Sarantopoulos J, et al. A phase II study of the c-Met RTK inhibitor XL880 in patients (pts) with papillary renal-cell carcinoma (PRC) [abstract]. J Clin Oncol 2007;25 Suppl:658s.

17. Jayson GC, Parker GJ, Mullamitha S, et al. Blockade of platelet-derived growth factor receptor-β by CDP860, a humanized, PEGylated di-Fab′, leads to fluid accumulation and is associated with increased tumor vascularized volume. J Clin Oncol 2005;23: 973–81.

18. Xian X, Håkansson J, Ståhlberg A, et al. Pericytes limit tumor cell metastasis. J Clin Invest 2006;116: 642–51.

19. Liu G, Rugo HS, Wilding G, et al. Dynamic contrast-enhanced magnetic resonance imaging as a pharmacodynamic measure of response after acute dosing of AG-013736, an oral angiogenesis inhibitor, in patients with advanced solid tumors: results from a phase I study. J Clin Oncol 2005;23:5464–73.

20. Wilmes LJ, Pallavicini MG, Fleming LM, et al. AG-013736, a novel inhibitor of VEGF receptor tyrosine kinases, inhibits breast cancer growth and decreases vascular permeability as detected by dynamic contrast-enhanced magnetic resonance imaging. J Magn Reson Imaging 2007;25:319–27.

21. Li KL, Wilmes LJ, Henry RG, et al. Heterogeneity in the angiogenic response of a BT474 human breast cancer to a novel vascular endothelial growth factor-receptor tyrosine kinase inhibitor: assessment by voxel analysis of dynamic contrast-enhanced MRI. J Magn Reson Imaging 2005;22:511–9.

22. Rixe O, Bukowski RM, Michaelson MD, et al. Axitinib treatment in patients with cytokine-refractory metastatic renal-cell cancer: a phase II study. Lancet Oncol 2007;8:975–84.

23. Cohen EEW, Rosen LS, Vokes EE, et al. Axitinib (AG-013736) is an active treatment for all histological subtypes of advanced thyroid cancer: results from a phase II study. J Clin Oncol 2008;26:4708–13.

24. Schiller JH, Larson T, Ou SI, et al. Efficacy and safety of axitinib (AG-013736; AG) in patients (pts) with advanced non-small cell lung cancer (NSCLC): a phase II trial [abstract]. J Clin Oncol 2007;25:386s.

25. Fruehauf JP, Lutzky J, McDermott DF, et al. Axitinib (AG-013736) in patients with metastatic melanoma: a phase II study [abstract]. J Clin Oncol 2008;26:484s.

26. Spano J, Chodkiewicz C, Maurel J, et al. Efficacy of gemcitabine plus axitinib compared with gemcitabine alone in patients with advanced pancreatic cancer: an open-label randomised phase II study. Lancet 2008; 317:2101–8.

27. Mendel DB, Laird AD, Xin X, et al. *In vivo* antitumor activity of SU11248, a novel tyrosine kinase inhibitor targeting vascular endothelial growth factor and platelet-derived growth factor receptors: determination of a pharmacokinetic/pharmacodynamic relationship. Clin Cancer Res 2003;9:327–37.

28. Waltenberger J, Claesson-Welsh L, Siegbahn A, Shibuya M, Heldin CH. Different signal transduction properties of KDR and Flt1, two receptors for vascular endothelial growth factor. J Biol Chem 1994;269: 26988–95.

29. Roberts WG, Whalen PM, Soderstrom E, et al. Antiangiogenic and antitumor activity of a selective PDGFR tyrosine kinase inhibitor, CP-673,451. Cancer Res 2005;65:957–66.

30. Miles AA, Miles EM. Vascular reactions to histamine, histamine-liberator and leukotaxine in the skin of guinea-pigs. J Physiol 1952;118:228–57.

31. Hoffman RM. Orthotopic metastatic mouse models for anticancer drug discovery and evaluation: a bridge to the clinic. J Invest New Drugs 1999;17: 343–60.

32. Jenkins DE, Hornig YS, Oei Y, Dusich J, Purchio T. Bioluminescent human breast cancer cell lines that permit rapid and sensitive *in vivo* detection of mammary tumors and multiple metastases in immune deficient mice. Breast Cancer Res 2005;7:R444–54.

33. Kroll J, Waltenberger J. A novel function of VEGF receptor-2 (KDR): rapid release of nitric oxide in response to VEGF-A stimulation in endothelial cells. Biochem Biophys Res Commun 1999;265:636–9.

34. Shiojima I, Walsh K. Role of Akt signaling in vascular homeostasis and angiogenesis. Circ Res 2002;90: 1243–50.

35. Rini BI, Schiller JH, Fruehauf JP, et al. Association of diastolic blood pressure (dBP) >90 mmHg with overall survival (OS) in patients treated with axitinib (AG-013736) [abstract]. J Clin Oncol 2008;26 Suppl:163.

36. Mancuso MR, Davis R, Norberg SM, et al. Rapid vascular regrowth in tumors after reversal of VEGF inhibition. J Clin Invest 2006;116:2610–21.

37. Inai T, Mancuso M, Hashizume H, et al. Inhibition of vascular endothelial growth factor (VEGF) signaling in cancer causes loss of endothelial fenestrations, regression of tumor vessels, and appearance of basement membrane ghosts. Am J Pathol 2004;165: 35–52.

38. Gunningham SP, Currie MJ, Han C, et al. Vascular endothelial growth factor-B and vascular endothelial growth factor-C expression in renal cell carcinomas: regulation by the von Hippel-Lindau gene and hypoxia. Cancer Res 2001;61:3206–11.

39. Alitalo K, Carmeliet P. Molecular mechanisms of lymphangiogenesis in health and disease. Cancer Cell 2002;1:219–27.

40. Jimenez X, Lu D, Brennan L, et al. A recombinant, fully human, bispecific antibody neutralizes the biological activities mediated by both vascular endothelial growth factor receptors 2 and 3. Mol Cancer Ther 2005;4:427–34.

41. Lyden D, Hattori K, Dias S, et al. Impaired recruitment of bone-marrow-derived endothelial and hematopoietic precursor cells blocks tumor angiogenesis and growth. Nat Med 2001;7:1194–201.

42. Stacker SA, Caesar C, Baldwin ME, et al. VEGF-D promotes the metastatic spread of tumor cells via the lymphatics. Nat Med 2001;7:186–91.

43. Kiba A, Sagara H, Hara T, Shibuya M. VEGFR-2-specific ligand VEGF-E induces non-edematous hyper-vascularization in mice. Biochem Biophys Res Commun 2003;301:371–7.

44. Laakkonen P, Waltari M, Holopainen T, et al. Vascular endothelial growth factor receptor 3 is involved in tumor angiogenesis and growth. Cancer Res 2007;67: 593–9.

45. Zheng Y, Murakami M, Takahashi H, et al. Chimeric VEGF-E(NZ7)/PlGF promotes angiogenesis via VEGFR-2 without significant enhancement of vascular permeability and inflammation. Arterioscler Thromb Vasc Biol 2006;26:2019–26.

46. Carmeliet P, Moons L, Luttun A, et al. Synergism between vascular endothelial growth factor and placental growth factor contributes to angiogenesis and plasma extravasation in pathological conditions. Nat Med 2001;7:575–83.

47. Autiero M, Waltenberger J, Communi D, et al. Role of PlGF in the intra- and intermolecular cross talk between the VEGF receptors Flt1 and Flk1. Nat Med 2003;9:936–43.

48. Whitaker GB, Limberg BJ, Rosenbaum JS. Vascular endothelial growth factor receptor-2 and neuropilin-1 form a receptor complex that is responsible for the differential signaling potency of VEGF(165) and VEGF(121). J Biol Chem 2001;276:25520–31.

49. Lee S, Chen TT, Barber CL, et al. Autocrine VEGF signaling is required for vascular homeostasis. Cell 2007;130:691–703.